Experimental verification of charge soliton excitations in the ionic Mott-Peierls ferroelectric TTF-CA

R. Takehara [1,*] H. Adachi [1] K. Sunami [1,†] K. Miyagawa [1] T. Miyamoto [2] H. Okamoto [2,3] S. Horiuchi [4] and K. Kanoda [1,‡]

[1]*Department of Applied Physics, University of Tokyo, Bunkyo-ku, Tokyo 113-8656, Japan*

[2]*Department of Advanced Materials Science, University of Tokyo, Kashiwa, Chiba 277-8561, Japan*

[3]*AIST-UTokyo Advanced Operando-Measurement Technology Open Innovation Laboratory (OPERANDO-OIL), National Institute of Advanced Industrial Science and Technology (AIST), Chiba 277-8568, Japan*

[4]*Research Institute for Advanced Electronics and Photonics (RIAEP), National Institute of Advanced Industrial Science and Technology (AIST), Tsukuba, Ibaraki 305-8565, Japan*

(Received 14 December 2021; accepted 8 March 2023; published 30 March 2023)

Strong coupling of charge, spin, and lattice in solids brings about emergent elementary excitations with their intertwining and, in one dimension, solitons are known as such. The charge-transferred organic ferroelectric, TTF-CA, has been argued to host charge solitons; however, the existence of the charge solitons remains unverified. Here, we demonstrate that the charge-transport gap in the ionic Mott-Peierls insulating phase of TTF-CA is an order of magnitude smaller than expected from quasiparticle excitations, however, being entirely consistent with the charge soliton excitations. We further suggest that charge and spin solitons move with similar diffusion coefficients in accordance with their coexistence. These results provide a basis for the thermal excitations of the emergent solitons.

DOI: 10.1103/PhysRevB.107.125164

I. INTRODUCTION

Topological excitations in one dimension (1D) are zero-dimensional defects behaving like particles. They are known as solitons and domain walls, which occasionally cause unconventional electrical and magnetic properties [1–12]. Notably, in the neutral-ionic (NI) transition material, TTF-CA, solitons are expected to emerge as elementary excitations responsible for electrical and magnetic properties in a strongly charge-spin-lattice-coupled Mott-Peierls system [13–15] and carry fractional charge [16–18].

In TTF-CA, an electron donor (D) molecule, TTF, and an acceptor (A) molecule, CA, alternately stack one-dimensionally and afford three phases as shown in Fig. 1 [12,19–21]. With applying pressure or lowering temperature, the neutral TTF-CA crystal progressively gains D-A electrostatic energy and then transitions or crosses over to an ionic Mott state by a charge transfer from TTF to CA [20,22]. Ionicity is measured by the degree of charge transfer, ρ, which is represented by $\rho_{\mathrm{N}} \sim 0.25$ in the neutral state and $\rho_{\mathrm{I}} \sim 0.75$ in the ionic Mott state [23–29]. Additionally, strong electron-lattice interactions cause static (dynamical) lattice dimerization along the 1D chain in a ferroelectric (paraelectric) ionic phase, denoted as I_{ferro} (I_{para}) phase hereafter, by Peierls or spin-Peierls mechanism (Fig. 1) [20,21,30,31]. In the I_{ferro} phase, the dimerization of TTF and CA is three-dimensional (3D) ferroelectric long-range ordered, whereas, in the I_{para} phase, thermal fluctuation of the dimerization breaks the long-range order, forming a dimer liquid state [11,21]. The phase of particular interest in the present work is this I_{para} phase located at high pressures and temperatures.

In general, the resistivity of organic semiconductors substantially decreases with pressure increased to several kilobars [32]. However, in the I_{para} phase of TTF-CA, the resistivity at room temperature is insensitive to pressure in a vast pressure region from 20 kbar at least up to 80 kbar [33]. Significantly, the I_{para} phase is suggested to host two types of solitons, charge and spin solitons, on the boundaries of the oppositely polarized domains (Fig. 1), both of which are predicted to contribute to electrical conduction [12–15]. The pressure-insensitive electrical conductivity possibly stems from the peculiar nature of the solitons; however, the existence of the charge soliton has not yet been experimentally verified. In the present work, to get its experimental evidence, we have investigated the temperature and pressure dependence of electrical resistivity of TTF-CA. To illustrate the peculiar electrical transport nature of TTF-CA under pressure, we have also investigated, as a reference system, the similar ionic material, TTF-BA, a nearly fully charge-transferred Mott insulator with ρ_{I} of ~0.95 [34–36], in which the charge degrees of freedom is strongly suppressed. The comparison of the two systems brings to light the existence of thermally excited solitons and their contribution to electrical conduction.

*Present address: Laboratory for Chemistry and Life Science, Institute of Innovative Research, Tokyo Institute of Technology, 4259 Nagatsuta, Midori-ku, Yokohama 226-8503, Japan; corresponding author: takehara.r.ab@m.titech.ac.jp

†Present address: Research Institute for Advanced Electronics and Photonics (RIAEP), National Institute of Advanced Industrial Science and Technology (AIST), Tsukuba, Ibaraki 305-8565, Japan.

‡Corresponding author: kanoda@ap.t.u-tokyo.ac.jp

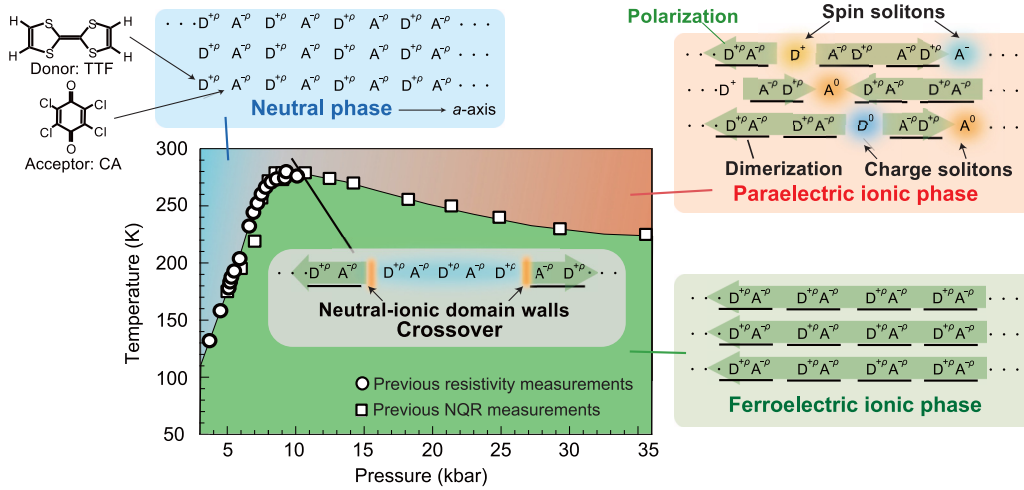

FIG. 1. Phase diagram of TTF-CA and schematic illustrations of the N, $I_{\rm para}$, and $I_{\rm ferro}$ phases with the charge transfer indicated by ρ and the polarization of dimers pointed out by bold green arrows. The phase diagram is reproduced from Ref. [12]. Mobile charge and spin solitons appear in the $I_{\rm para}$ phase. In the crossover between the N and $I_{\rm para}$ phases, NI domain walls are excited.

II. EXPERIMENT

We performed the electrical resistivity measurements for TTF-CA and TTF-BA under pressure with the four-terminal method. The electrical current was injected along the 1D chains, namely, the a axis for TTF-CA and the b axis for TTF-BA. The samples were mounted in a clamp-type piston-cylinder pressure cell, and Daphne 7373 and 7474 oils were used as the pressure-transmitting media up to 20 and 35 kbar, respectively, where pressure is hydrostatic [37]. The pressure values quoted in this paper indicate internal pressures that were reduced from external pressures by the pressure-efficiency factor of 0.9 determined separately with a Manganin wire used as an indicator of the internal pressure.

III. RESULTS AND DISCUSSION

A. Pressure dependence of resistivity of TTF-CA and TTF-BA

Figure 2(a) compares the pressure dependences of the resistivities of TTF-CA and TTF-BA at room temperature (the data for pressures below 20 kbar in TTF-CA are reproduced from Ref. [12]). With increasing pressure, the resistivity of TTF-CA takes a minimum at 8–9 kbar and levels off to a value of ∼2.5 Ω cm above 20 kbar. Our previous study demonstrated that the resistivity minimum results from the NI domain wall (NIDW) excitations arising around NI crossover pressure (Fig. 1) [12]. The present experiment with the piston-cylinder pressure cell confirmed the pressure-insensitive resistivity previously suggested by the experiment using the cubic anvil apparatus [33]. Contrastingly, the resistivity of TTF-BA is as high as ∼1 Ω cm, which shows a little sensitivity to pressure in the entire pressure range studied. Remarkably, the resistivity values are five to six orders of magnitude different between the two systems at high pressures despite that both are commonly in the $I_{\rm para}$ phase.

B. Temperature dependence of electrical resistivity of TTF-CA and TTF-BA

We show the Arrhenius plots of the resistivities of TTF-BA and TTF-CA in Figs. 2(b) and 2(c), respectively [part of the data in Fig. 2(c) is reproduced from Ref. [12]]. The resistivity of TTF-BA is characterized by the activation energies of 0.38–0.42 eV at every pressure up to 35 kbar [the inset of Fig. 2(b)]. The charge soliton excitation expected in the NI transition materials is akin to a neutral single-molecule defect (Fig. 1), whose excitation energy is predicted to be an order of magnitude smaller than the charge-transfer (CT) energy gap [13–15]. In TTF-BA, however, the charge gap, which is twice the activation energy, is nearly equal to the CT energy of ∼0.8 eV determined by the IR measurements [34], which is consistent with quasiparticle excitations over the Mott gap and rules out the solitonic excitations in TTF-BA. The small decrease in the charge gap above 25 kbar is ascribable to an increase of the transfer integral. On the other hand, the small increase up to 25 kbar may be due to the stabilization of the ionic state owing to a Madelung energy gain by lattice contraction.

The five to six orders of magnitude smaller resistivity in TTF-CA than in TTF-BA [Fig. 2(a)] suggests that the $I_{\rm para}$ phase of TTF-CA has much lower charge excitation energy than that of CT or band quasiparticles. As seen in Fig. 2(c), the slope of the Arrhenius curve in the $I_{\rm para}$ phase gradually changes with pressure increased up to 20 kbar and is nearly unchanged above 20 kbar, which is more visible when the conductivity is normalized to the value at T_c as shown in the inset of Fig. 2(c). Figure 3(a) displays the activation energies estimated from the slope in the $I_{\rm para}$ phase, which is ∼0.26 eV at 10 kbar and drops to ∼0.10 eV at 20 kbar, then saturating to the range of 0.06–0.07 eV above 25 kbar.

This analysis, however, requires the following caution. The low resistivity of TTF-CA around 10 kbar [the red area in Fig. 3(b)] is caused by the excitations of the NIDWs [12]. As discussed in Ref. [12], the NI crossover region is inclined in the pressure-temperature ($P-T$) plane and the resistivity should be analyzed parallel to the tilted crossover line in the NIDW-active $P-T$ region. The activation energies determined in this way [12], which are reproduced in Fig. 3(a), show large discrepancies with the above estimated activation energies below 20 kbar, thus, which should be taken as spurious values. On the other hand, the activation energy decreases

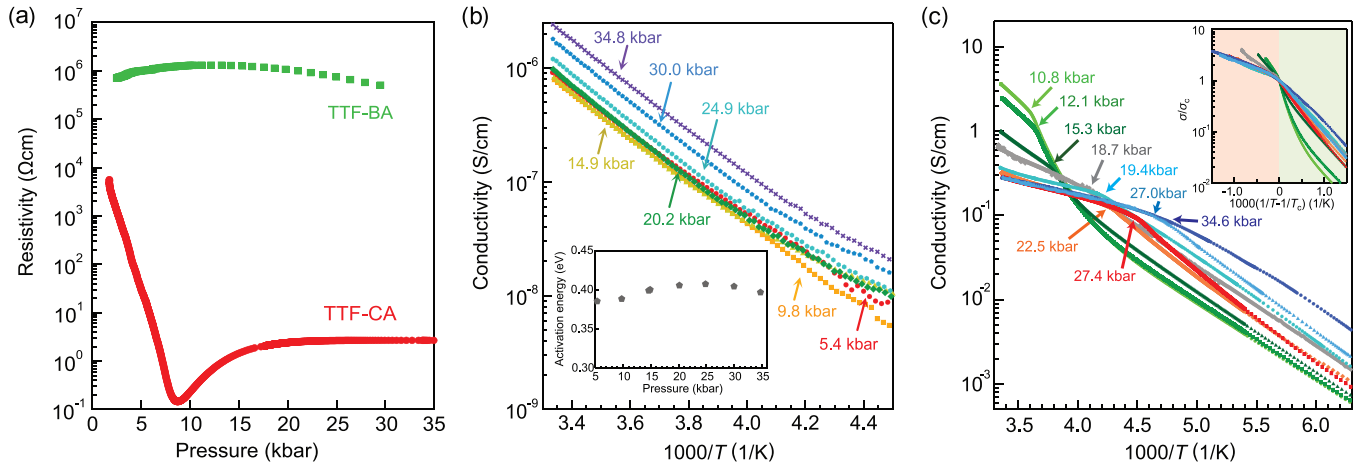

FIG. 2. (a) Comparison between the pressure dependence of the resistivities of TTF-CA along the a axis and TTF-BA along the b axis at room temperature (data for pressures below 20 kbar in TTF-CA are reproduced from Ref. [12]). (b) Arrhenius plot of the resistivity of TTF-BA along the b axis at several pressures. The conductivity totally decreases with increasing pressure up to 10–15 kbar but increases with further pressure increase. The inset shows the pressure dependence of activation energy of TTF-BA estimated from the Arrhenius plot. (c) Arrhenius plot of the resistivity of TTF-CA along the a axis at several pressures. Part of the data in Fig. 2(c) is reproduced from Ref. [12]. The arrows indicate the phase transition points, T_c, between the $I_{\rm para}$ and $I_{\rm ferro}$ phases. The inset shows the Arrhenius plot of the normalized conductivity σ/σ_c against $1000(1/T - 1/T_c)$, where σ_c is the conductivity at T_c. The red and green regions in the inset correspond to the $I_{\rm para}$ and $I_{\rm ferro}$ phases, respectively.

to 0.06–0.08 eV in the pressure range above 20 kbar, being the same order with those around 10 kbar. These values are far smaller than a half of the CT excitation energy [22] or the recently reported band gap, ∼0.35 eV [38], indicating the nonquasiparticle transport. In the $I_{\rm para}$ phase, where the 3D ferroelectric order is broken and the lattice fluctuation exists, there should not be an activation barrier for carriers to move. In fact, as shown in Fig. 1, the $I_{\rm para}$ phase is located in the temperature range above 230 K, where it is higher than the activation energy of 0.02 eV for the mobility in the $I_{\rm ferro}$ phase [39], suggesting that the mobility in the $I_{\rm para}$ phase is not an activation type. Therefore, the activation energy of 0.06–0.08 eV above 20 kbar should be the carrier generation energy. The free NIDW excitations should be suppressed above 20 kbar far from the NI crossover pressure; thus, these results demonstrate the existence of another low-energy excitation carrier, that is, the soliton whose activation energy is theoretically predicted to be less than 0.1 eV [13]. Overall, the activation energy of the NIDWs is considered to cross over to that of the solitons in a way depicted by the broad curve in Fig. 3(a); the NIDW excitation energy taking a minimum value, 0.055 eV, at 9 kbar [12] increases with pressure but gradually turns back to the similar value at high pressures though the soliton excitation energy should be over twice the NIDW excitation energy [13,15]. We speculate that local lattice deformation associated with the soliton formation may lower its creation energy; this is an issue of further investigation.

C. Analysis of the activation energy of charge soliton

In what follows, we make quantitative discussion on the observed activation energy of 0.06–0.08 eV. The NI transition system has been modeled to the form of the Hubbard-type Hamiltonian that includes the on-site repulsive energy, U, the intersite attractive energy, $-V$, and the site-alternating potential, Δ_0, reflecting the energy difference between the highest occupied molecular orbital of the D molecule and the lowest unoccupied molecular orbital of the A molecule [40]. This Hamiltonian is reduced to the extended Hubbard model with U, the repulsive V, and the reduced Δ $(= \Delta_0 - 4V)$, and is further transformed to a phase Hamiltonian through the bosonization [41]. The analytical solution of the energy of charge soliton, $E_{\rm CS}$, was obtained by Fukuyama and Ogata [14] as

$$E_{\rm CS} = \frac{2v_\rho\sqrt{\gamma_c}}{\pi}\left[\cos\theta - \sin\theta\left(\frac{\pi}{2} - \theta\right)\right], \qquad (1)$$

where $v_\rho = 2ta + (U + 6V)a/2\pi$, $\gamma_c = (U - 2V)/\pi a v_\rho$, a is the lattice constant, and t is the transfer integral between the D and A molecules. θ is a phase variable for charge that characterizes the degree of charge transfer from a D to A molecule; for example, θ is 0 and $\pi/2$ in the ionic and neutral limits, respectively. The charge soliton should be exactly neutral whereas the ionic background can have an intermediate charge transfer expressed by θ. Thus, the creation energy of a charge soliton in the ionic background solely depends on the θ value of the ionic phase and is given by Eq. (1).

The topological charge of the charge soliton, $q_{\rm CS}$, corresponds to the difference between the neutral charge and the background ionic charge and is experimentally estimated by $q_{\rm CS}/e = \pm\rho_{\rm I}$, which is related to θ through $q_{\rm CS}/e = 1 - 2\theta/\pi$ [15], where e is the elementary charge. The $q_{\rm CS}$ value of $0.75e$ in the $I_{\rm para}$ phase yields $\theta = 0.39$ and thus $\cos\theta - \sin\theta(\frac{\pi}{2} - \theta) = 0.47$. The v_ρ and γ_c are the functions of t and V that vary with pressure. Using the reported parameter sets of $(U, V, t) = (1.5, 0.7, 0.2)$ [13] and $(1.528, 0.604, 0.179)$ [42] in eV at ambient pressure and taking account of the pressure effect [11,43], we obtained $v_\rho\gamma_c^{1/2}$ at 20 kbar as 0.13 and 0.34,

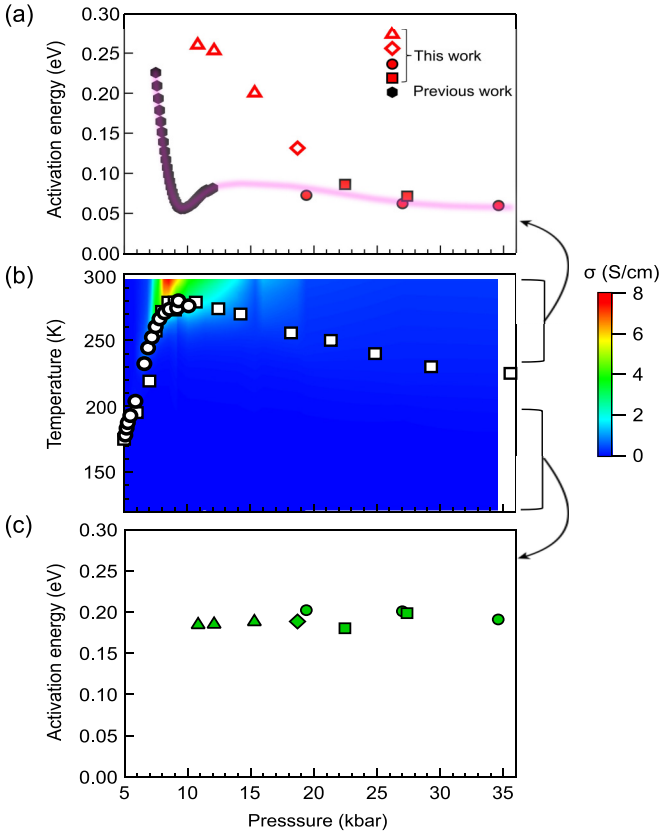

FIG. 3. (a) Pressure dependence of the activation energy of TTF-CA in the high-temperature region above the ferroelectric transition temperature, T_c. The results of four samples measured are distinguished by the different symbols. The activation energies are obtained from the plots in Fig. 2(c). The activation energies estimated along parallel to the inclined NI crossover line in the previous measurements [12] are also displayed. The pressure dependence of activation energy that appears to make sense is indicated by the guided curve. (b) Phase diagram of TTF-CA with the contour plot of electrical conductivity, σ, along the a axis extracted from Ref. [12]. (c) Pressure dependence of activation energy of TTF-CA in the I_{ferro} phase.

which yield E_{CS} of 0.04 and 0.1 eV, respectively. The range of these values explains the experimental values of 0.06–0.08 eV, lending support to the view that the charge soliton dominates the electric conduction in the I_{para} phase.

The solitonic electrical conduction is featured by little pressure dependence of activation energy as shown in Fig. 3(a). ρ_{I} is known to be nearly pressure-independent in the I_{para} phase [21,24,26,28,29], meaning that θ is so as well. The prefactor, $v_\rho \gamma_c^{1/2}$, in Eq. (1) is estimated to only vary by 1.6%/kbar and 0.1%/kbar for the two sets of (U, V, t) values used in the above estimation [13,42] according to the pressure effect [11,43]. This explains the pressure-insensitive activation energy at high pressures. More rigorously, the electron-phonon coupling, the many-body effects of solitons, and the quantum fluctuations beyond the present consideration may influence the E_{CS} value. As to the electron-phonon coupling, the E_{CS} values with and without the electron-phonon coupling are theoretically compared in Ref. [15], and are suggested to be quantitatively the same in the ionic state far from the NI boundary. In practice, there should also exist an electron-molecule coupling that leads to an intramolecular deformation. This effect would modify the soliton excitation energy.

D. Charge soliton density and diffusion coefficient

Next, we discuss the diffusion dynamics of charge solitons. The steady current of charge solitons requires the presence of spin solitons [13–15] as follows. A pair of charge solitons with $q_{\text{CS}}/e = +\rho_{\text{I}}$ and $-\rho_{\text{I}}$, thermally created in the ionic dimer configuration,...DA DA DA..., are recombined or dissociated, depending on whether the polarity of the soliton pair is parallel or antiparallel to the direction of an applied electric field. In case of dissociation, which causes an electrical current, the passing charge soliton inverts the DA dimers to AD ones in the ionic background. However, a pair of charge solitons subsequently created there become recombined. Thus, a steady current requires a turning of the AD dimers to the DA ones. This is attained by the creation of spin solitons having topological charge, $q_{\text{SS}} = \pm(1 - \rho_{\text{I}})e$ [15], oppositely signed to that of charge soliton, $q_{\text{CS}}/e = \pm\rho_{\text{I}}$; therefore, the spin solitons are dissolved and invert the dimer pattern. Thus, we take the effective charge of the carrier as $\pm e$ that is the sum of the topological charges of the charge and spin solitons, $q_{\text{CS}} = \pm\rho_{\text{I}}e$ and $q_{\text{SS}} = \pm(1 - \rho_{\text{I}})e$ [15]. Theoretically, the excitation energy of the charge soliton is suggested to be higher than that of the spin soliton [13–15], and thus the number of thermally excited charge solitons should be less than that of spin solitons. Although both the charge and spin solitons are responsible for electrical conduction, it is governed by the number of minority carriers, that is, the charge soliton. Therefore, the electrical conductivity is expressed as $\sigma = en_{\text{CS}}\mu_{\text{CS}}$, where n_{CS} and μ_{CS} are the density and mobility of charge soliton, respectively. Using the experimental value of $\sigma = 0.4$ S/cm at 20 kbar, we obtain $n_{\text{CS}}\mu_{\text{CS}} = 2.5 \times 10^{18}$ 1/V scm. As the charge soliton is equivalent to a pair of combined NIDWs sandwiching a neutral molecule (Fig. 1), μ_{CS} would be smaller than the mobility of the NIDW, which is estimated at $\mu_{\text{NIDW}} = 0.14\,\text{cm}^2/\text{V}\ \text{s}$ through $\sigma_{\text{NIDW}} = (e/2)n_{\text{NIDW}}\mu_{\text{NIDW}}$ with $\sigma_{\text{NIDW}} = 7$ S/cm and $n_{\text{NIDW}} \sim 6.1 \times 10^{20}$ 1/cm^3 (one soliton per approximately five DA pairs) at 9 kbar [12]. Assuming, e.g., $\mu_{\text{CS}} = \mu_{\text{NIDW}}/2 \sim 0.072$, we have the estimate of $n_{\text{CS}} \sim 3.5 \times 10^{19}$ 1/cm^3 (one soliton per ~88 DA pairs) at 20 kbar after a lattice contraction by 7% is considered [43]. This charge soliton density is several times smaller than the spin soliton density at 14 kbar, one soliton per 10–25 DA pairs [11]. This difference is reasonable because the charge soliton has larger excitation energy than the spin soliton. Then, the charge-soliton diffusion coefficient, D_{CS}, which is given by the Einstein relationship, $\mu_{\text{CS}} = eD_{\text{CS}}/k_{\text{B}}T$, is $\sim 1.9 \times 10^{-3}\text{cm}^2/\text{s}$ at 300 K, where k_{B} is the Boltzmann constant. On the other hand, the diffusion coefficient of spin soliton, D_{SS}, was previously evaluated by ^{1}H-NMR as $2.4 \times 10^{-3}\text{cm}^2/\text{s}$ at 14 kbar at 300 K [11]. It is surprising that the D_{CS} and D_{SS} values determined by completely different experimental methods nearly coincide with each other. This result indicates that the

charge and spin solitons move together, strongly supporting the theoretical prediction that the spin solitons are required as well as the charge solitons to carry steady current [13–15].

E. Electrical conduction in the low-temperature phase

As seen in Fig. 2(c), the Arrhenius plot of resistivity in the I_{ferro} phase of TTF-CA appears approximately parallel for every pressure above 10 kbar and is characterized by the activation energies of 0.18–0.21 eV, which are about three times as large as the E_{CS} values [Fig. 3(c)]. Nevertheless, the activation energies are smaller than a half of the CT energy, 0.35 eV, suggesting that the charge carriers in the I_{ferro} phase are not the band quasiparticles either. In fact, the previous conductivity, NMR, and NQR studies of the I_{ferro} phase at 14 kbar suggested that the charge (and spin) carrier should be a polaron [39]. The polaron is the combined excitation of a charge and a spin soliton, which does not break the three-dimensional ferroelectric order. Unlike the discontinuous transition from N to I_{ferro} phases at ambient pressure, the resistivity shows no jump at the I_{para} to I_{ferro} phase transition [Fig. 2(c)]. This nature supports the soliton binding picture of the I_{para} to I_{ferro} phase transition, which leads to the polaron formation [39], in contrast to the discontinuous transition caused by the simultaneous charge transfer and lattice dimerization under low pressures. The activation energy larger than that of the charge soliton is reasonable by considering the composite character of the polaron. According to the previous analysis, the mobility gap in the I_{ferro} phase, which also contributes to the activation energy in the polaron transport, was estimated at 0.02 eV [39]. Thus, the observed activation energy of 0.18–0.21 eV in charge transport is nearly determined by the polaron creation energy. Its pressure insensitivity reasonably accords with the pressure insensitivity of the charge soliton activation energy.

IV. CONCLUDING REMARKS

The present study has verified that the charge transport in the I_{para} phase is carried by charge solitons having the excitation energy of 0.06–0.08 eV, consistent with theoretical prediction [13]. In conjunction with the previous studies [11,12,39], it has made clear that different charge carriers are vital in different regions in the phase diagram (Fig. 1); that is, NIDWs around the N-I_{para} boundary, solitons in the I_{para} phase, and polarons in the I_{ferro} phase. The excitation energy of NIDWs emerging at the lower pressures smoothly approaches the charge soliton excitation energy with increasing pressure, where the neutral domains progressively shrink to single neutral molecules, namely, the charge solitons. We have also estimated the diffusion coefficient of a charge soliton and found it to roughly accord with that of a spin soliton, suggesting that they move together. The present results provide foundations on the thermal excitations of topological defects in a quasi-1D ionic Mott-Peierls ferroelectric. X-ray diffuse scattering and dielectric measurements are expected to provide further information on structural spatial correlations such as 1D structural fluctuations and polar fluctuations with soliton dynamics.

ACKNOWLEDGMENTS

We thank M. Tsuchiizu, H. Seo, and H. Fukuyama for fruitful discussions. This work was supported by the JSPS Grant-in-Aids for Scientific Research (Grants No. JP18H05225, No. 20K20894, No. 20KK0060, No. 21H04988, and No. 21K18144), and by CREST (Grant No. JPMJCR1661), Japan Science and Technology Agency. We also thank the Cryogenic Research Center at the University of Tokyo for supporting low-temperature experiments.

[1] B. R. Weinberger, E. Ehrenfreund, A. Pron, A. J. Heeger, and A. G. MacDiarmid, J. Chem. Phys. **72**, 4749 (1980).
[2] A. J. Heeger, S. Kivelson, J. R. Schrieffer, and W. P. Su, Rev. Mod. Phys. **60**, 781 (1988).
[3] T. Mitani, G. Saito, Y. Tokura, and T. Koda, Phys. Rev. Lett. **53**, 842 (1984).
[4] T. Mitani, Y. Kaneko, S. Tanuma, Y. Tokura, T. Koda, and G. Saito, Phys. Rev. B **35**, 427 (1987).
[5] Y. Tokura, H. Okamoto, T. Koda, T. Mitani, and G. Saito, Phys. Rev. B **38**, 2215 (1988).
[6] H. Okamoto, T. Komatsu, Y. Iwasa, T. Koda, Y. Tokura, S. Koshihara, T. Mitani, and G. Saito, Synth. Met. **27**, 189 (1988).
[7] Y. Iwasa, T. Koda, Y. Tokura, S. Koshihara, N. Iwasawa, and G. Saito, Appl. Phys. Lett. **55**, 2111 (1989).
[8] Y. Tokura, S. Koshihara, Y. Iwasa, H. Okamoto, T. Komatsu, T. Koda, N. Iwasawa, and G. Saito, Phys. Rev. Lett. **63**, 2405 (1989).
[9] H. Okamoto, T. Mitani, Y. Tokura, S. Koshihara, T. Komatsu, Y. Iwasa, T. Koda, and G. Saito, Phys. Rev. B **43**, 8224 (1991).
[10] N. Kirova, S. Brazovskii, A. Choi, and Y. W. Park, Phys. B: Condens. Matter **407**, 1939 (2012).
[11] K. Sunami, T. Nishikawa, K. Miyagawa, S. Horiuchi, R. Kato, T. Miyamoto, H. Okamoto, and K. Kanoda, Sci. Adv. **4**, eaau7725 (2018).
[12] R. Takehara, K. Sunami, K. Miyagawa, T. Miyamoto, H. Okamoto, S. Horiuchi, R. Kato, and K. Kanoda, Sci. Adv. **5**, eaax8720 (2019).
[13] N. Nagaosa, J. Phys. Soc. Jpn. **55**, 2754 (1986).
[14] H. Fukuyama and M. Ogata, J. Phys. Soc. Jpn. **85**, 023702 (2016).
[15] M. Tsuchiizu, H. Yoshioka, and H. Seo, J. Phys. Soc. Jpn. **85**, 104705 (2016).
[16] R. E. Prange, Phys. Rev. B **26**, 991 (1982).
[17] D. J. Thouless, Phys. Rev. B **27**, 6083 (1983).
[18] N. Kirova and S. Brazovskii, Phys. B: Condens. Matter **404**, 382 (2009).
[19] M. Le Cointe, M. H. Lemée-Cailleau, H. Cailleau, B. Toudic, L. Toupet, G. Heger, F. Moussa, P. Schweiss, K. H. Kraft, and N. Karl, Phys. Rev. B **51**, 3374 (1995).
[20] M. Cointe, E. Collet, B. Toudic, P. Czarnecki, and H. Cailleau, Crystals **7**, 285 (2017).

[21] R. Takehara, K. Sunami, F. Iwase, M. Hosoda, K. Miyagawa, T. Miyamoto, H. Okamoto, and K. Kanoda, Phys. Rev. B **98**, 054103 (2018).
[22] J. B. Torrance, J. E. Vazquez, J. J. Mayerle, and V. Y. Lee, Phys. Rev. Lett. **46**, 253 (1981).
[23] A. Girlando, F. Marzola, C. Pecile, and J. B. Torrance, J. Chem. Phys. **79**, 1075 (1983).
[24] Y. Tokura, H. Okamoto, T. Koda, and T. Mitani, Solid State Commun. **57**, 607 (1986).
[25] M. Hanfland, A. Brillante, A. Girlando, and K. Syassen, Phys. Rev. B **38**, 1456 (1988).
[26] H. Matsuzaki, H. Takamatsu, H. Kishida, and H. Okamoto, J. Phys. Soc. Jpn. **74**, 2925 (2005).
[27] S. Horiuchi, R. Kumai, Y. Okimoto, and Y. Tokura, Chem. Phys. **325**, 78 (2006).
[28] M. Masino, A. Girlando, and A. Brillante, Phys. Rev. B **76**, 064114 (2007).
[29] A. Dengl, R. Beyer, T. Peterseim, T. Ivek, G. Untereiner, and M. Dressel, J. Chem. Phys. **140**, 244511 (2014).
[30] M. H. Lemée-Cailleau, M. Le Cointe, H. Cailleau, T. Luty, F. Moussa, J. Roos, D. Brinkmann, B. Toudic, C. Ayache, and N. Karl, Phys. Rev. Lett. **79**, 1690 (1997).
[31] T. Luty, H. Cailleau, S. Koshihara, E. Collet, M. Takesada, M. H. Lemée-Cailleau, M. Buron-Le Cointe, N. Nagaosa, Y. Tokura, E. Zienkiewicz, and B. Ouladdiaf, Europhys. Lett. **59**, 619 (2002).
[32] Y. Kurosaki, Y. Shimizu, K. Miyagawa, K. Kanoda, and G. Saito, Phys. Rev. Lett. **95**, 177001 (2005).
[33] R. Takehara, K. Miyagawa, K. Kanoda, T. Miyamoto, H. Matsuzaki, H. Okamoto, H. Taniguchi, K. Matsubayashi, and Y. Uwatoko, Phys. B: Condens. Matter **460**, 83 (2015).
[34] A. Girlando, C. Pecile, and J. B. Torrance, Solid State Commun. **54**, 753 (1985).
[35] P. García, S. Dahaoui, P. Fertey, E. Wenger, and C. Lecomte, Phys. Rev. B **72**, 104115 (2005).
[36] F. Delchiaro, A. Girlando, A. Painelli, A. Bandyopadhyay, S. K. Pati, and G. D'Avino, Phys. Rev. B **95**, 155125 (2017).
[37] K. Murata, K. Yokogawa, H. Yoshino, S. Klotz, P. Munsch, A. Irizawa, M. Nishiyama, K. Iizuka, T. Nanba, T. Okada, Y. Shiraga, and S. Aoyama, Rev. Sci. Instrum. **79**, 085101 (2008).
[38] V. Borisov, S. Biswas, Y. Li, and R. Valenti, Phys. Status Solidi B **256**, 1900229 (2019).
[39] K. Sunami, R. Takehara, A. Katougi, K. Miyagawa, S. Horiuchi, R. Kato, T. Miyamoto, H. Okamoto, and K. Kanoda, Phys. Rev. B **103**, 134112 (2021).
[40] N. Nagaosa, J. Phys. Soc. Jpn. **55**, 2745 (1986).
[41] J. Hara and H. Fukuyama, J. Phys. Soc. Jpn. **52**, 2128 (1983).
[42] K. Yonemitsu, Phys. Rev. B **73**, 155120 (2006).
[43] R. M. Metzger and J. B. Torrance, J. Am. Chem. Soc. **107**, 117 (1985).